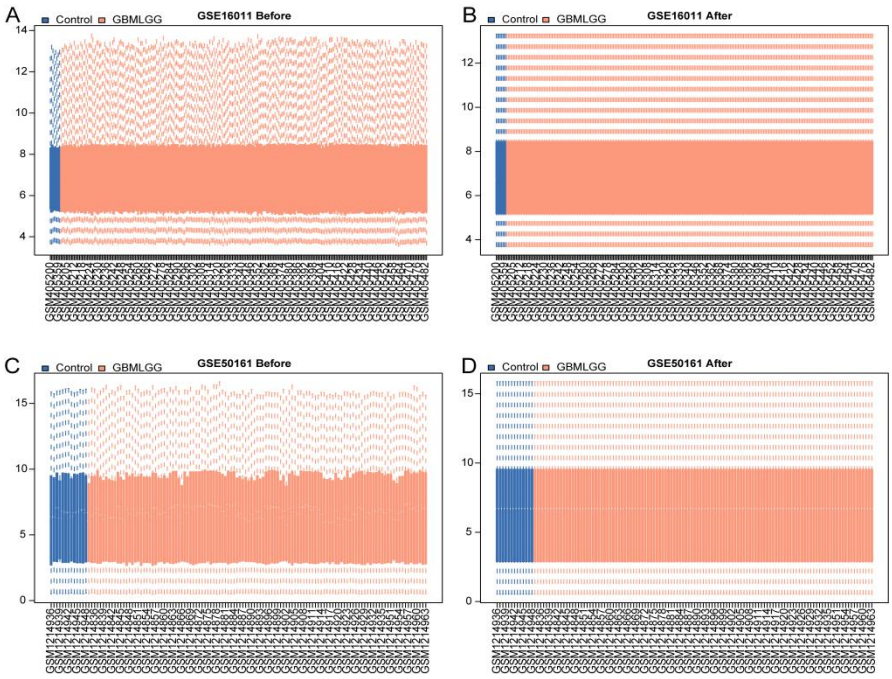

Fig.S1 Data preprocessing

(A) The boxplot of dataset GSE16011 before batch processing. (B) The boxplot of dataset GSE16011 after batch processing. (C) The boxplot of dataset GSE50161 before batch processing. (D) The boxplot of dataset GSE50161 after batch processing.

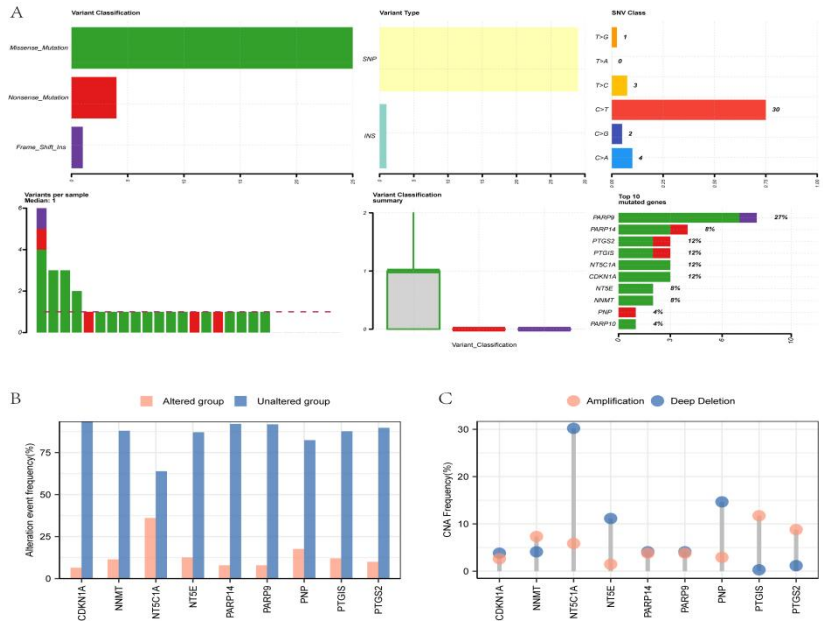

Fig.S2 Mutation analysis and copy number variation of hub genes

(A) Mutation analysis of hub genes in GBMLGG patients in the TCGA-GBMLGG dataset. (B) Group comparison chart of copy number variation of hub genes in GBMLGG patients in the TCGA-GBMLGG dataset. (C) Group comparison chart of

copy number alteration types of hub genes in GBMLGG patients in the TCGA-GBMLGG dataset.

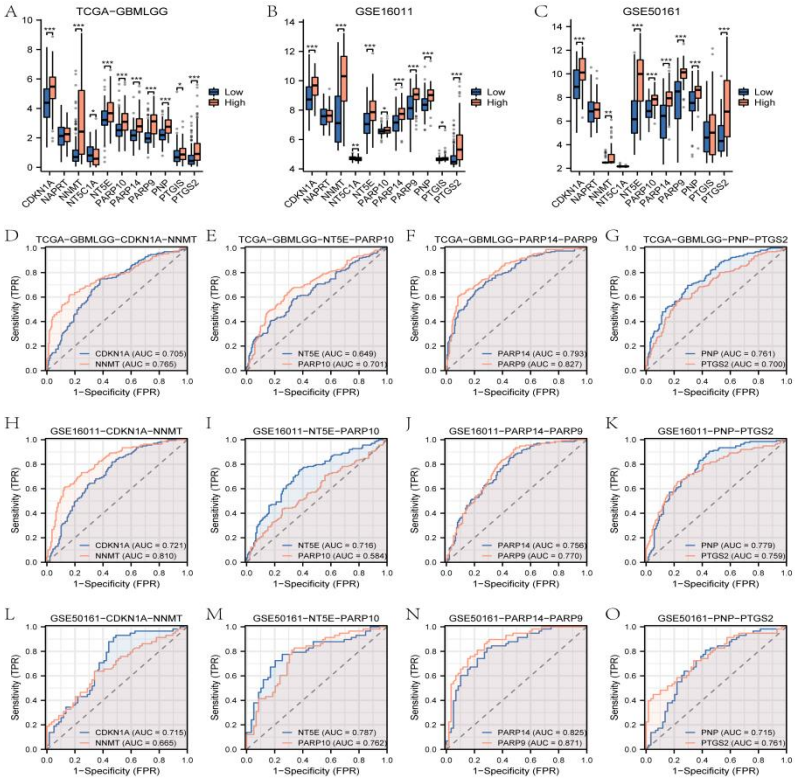

Fig. S3 Differential expression analysis of hub genes between the high- and low-NAMs groups in the TCGA-GBMLGG, GSE16011, and GSE50161 datasets

(A) Comparison chart of hub genes in TCGA-GBMLGG dataset between the high- and low-NAMs groups. (B) Comparison chart of hub genes between high- and low-NAMs groups in the GSE16011 dataset. (C) Group comparison chart of hub genes between high and low groups of NAMs in the GSE50161 dataset. (D-G) Hub genes CDKN1A (D blue line), NNMT (D red line), NT5E (E blue line), PARP10 (E red line), PARP14 (F blue line), PARP9 (F red line), PNP (G blue line), and the ROC curve results of PTGS2 (G red line) in the TCGA-GBMLGG data set are displayed. (H-K) Hub genes CDKN1A (H blue line), NNMT (H red line), NT5E (I blue line), PARP10 (I red line), PARP14 (J blue line), PARP9 (J red line), PNP (K blue line), and the ROC curve results of PTGS2 (K red line) in the GSE16011 data set are displayed. (L-O) Hub genes CDKN1A (L blue line), NNMT (L red line), NT5E (M blue line), PARP10 (M red line), PARP14 (N blue line), PARP9 (N red line), PNP (O blue line), and the ROC curve results of PTGS2 (O red line) in the GSE50161 data set are

displayed. *P < 0.05, **P < 0.01, ***P < 0.001. ROC curves with AUC values closer to 1 indicate better diagnostic accuracy. AUC values between 0.5-0.7 indicate low accuracy, and AUC values between 0.7-0.9 indicate moderate accuracy.

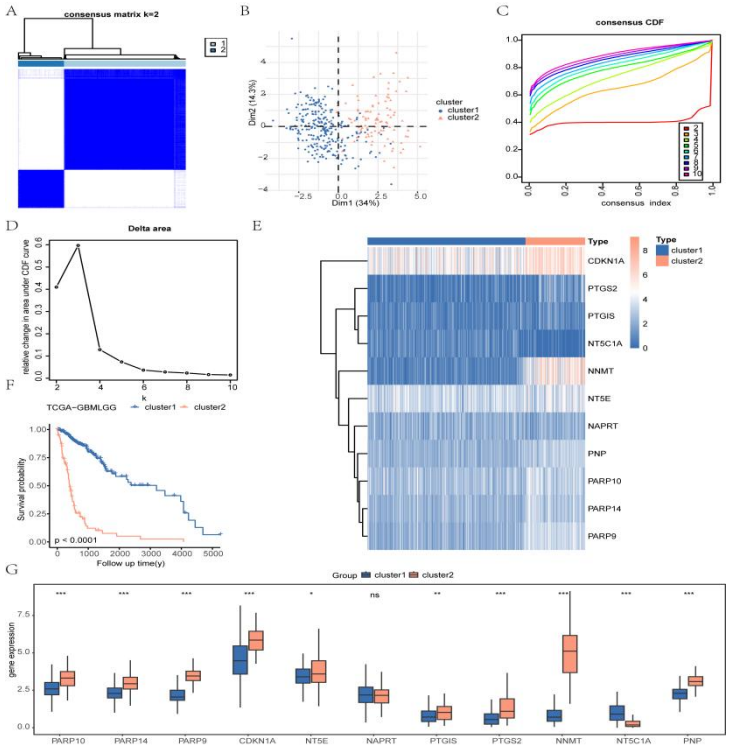

Fig. S4 Construction of related subtypes of GBMLGG

(A) The consensus clustering (K=2) result plot pertains to GBMLGG in the TCGA-GBMLGG dataset. (B) PCA analysis results of two GBMLGG disease subtypes (cluster1 and cluster2) in the TCGA-GBMLGG dataset. (C-D) Consistency cluster cumulative distribution function (CDF) plot (C) and area under the CDF curve Delta plot (D) for different numbers of clusters in the consensus cluster. (E) Heat map display of the expression of hub genes in different GBMLGG subtypes. (F) The prognostic KM curve analysis results of two GBMLGG subtypes (cluster1 and cluster2) in the TCGA-GBMLGG data set are displayed. (G) Group comparison diagram of hub genes in different GBMLGG subtypes in the TCGA-GBMLGG dataset. ns P ≥ 0.05, * P < 0.05, **P < 0.01, ***P < 0.001.

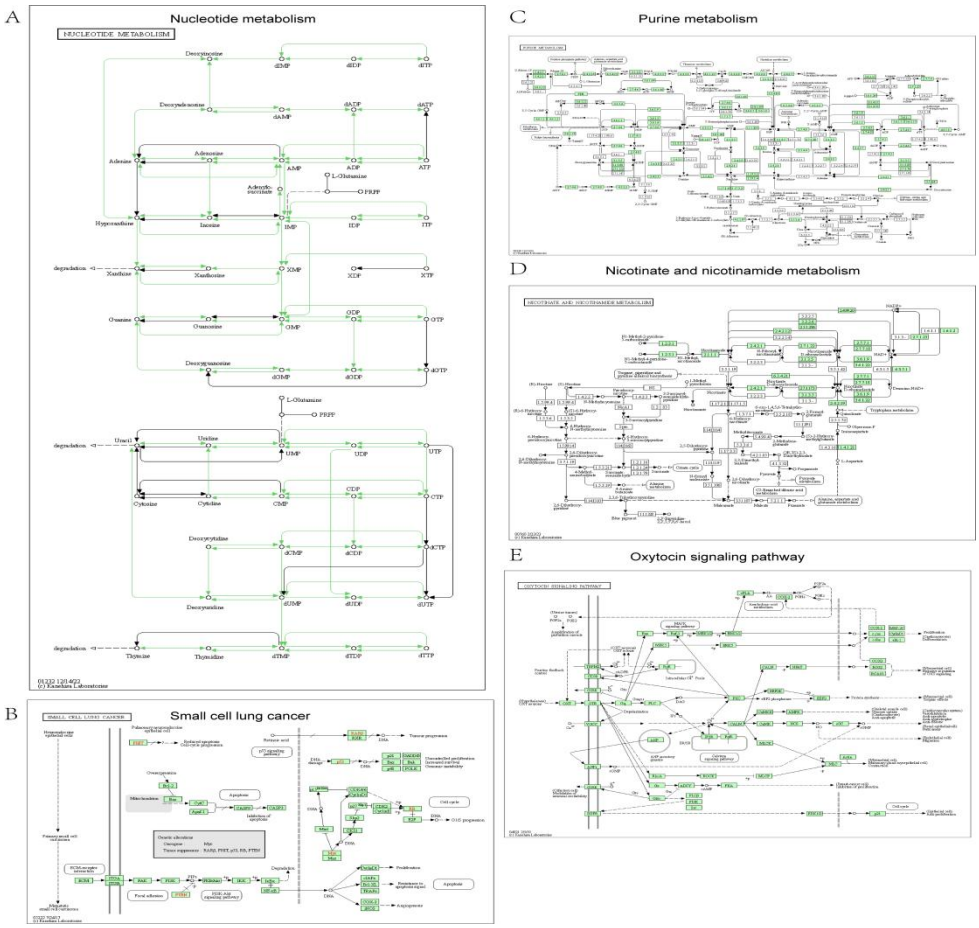

Fig. S5 KEGG pathway enrichment analysis of key genes

(A-E) KEGG pathway enrichment analysis results of key genesare presented in the form of a graph, (including Nucleotide metabolism (A), Small cell lung cancer (B), Purine metabolism (C), Nicotinate and nicotinamide metabolism (D), Oxytocin signaling pathway (E)). The screening criteria for KEGG enrichment items were P.adj < 0.05 and FDR value (*q.value*) < 0.05.

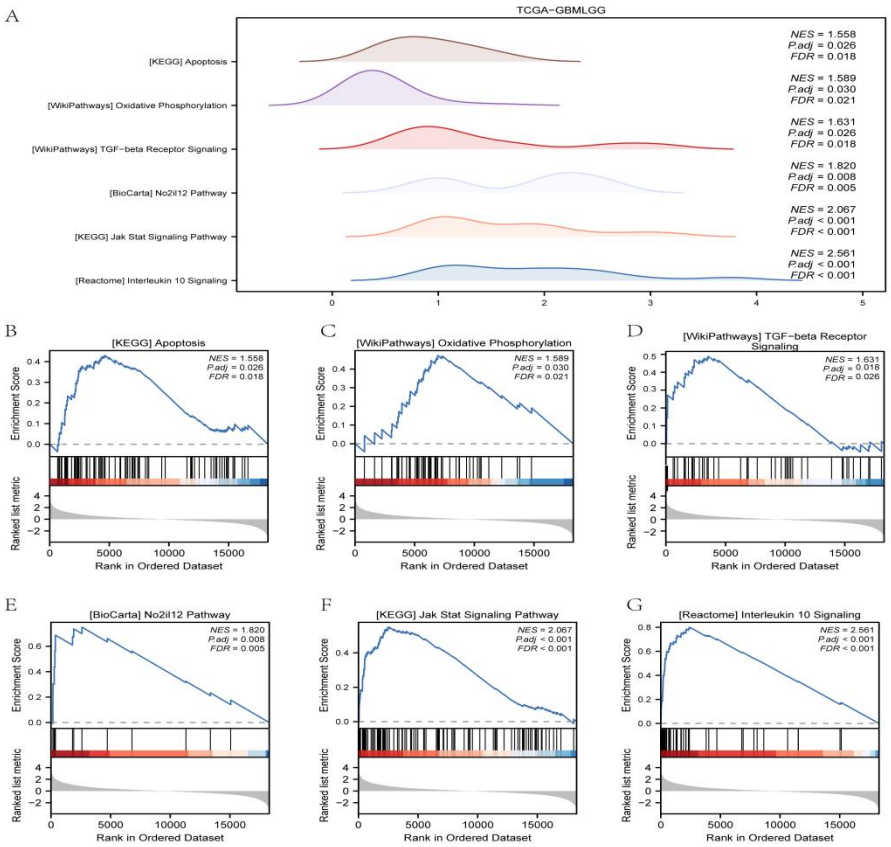

Fig. S6 GSEA enrichment analysis between high- and low-risk groups in key genes prognostic model.

(A) TCGA-GBMLGG data set key genes prognostic model GSEA enrichment analysis of genes between high- and low-risk groups mainly six biological characteristics. (B–G) Genes are significantly enriched in apoptosis (B), oxidative phosphorylation (C), Tgfbeta receptor signaling (D), NO2IL12 pathway (E), JAK-STAT signaling pathway (F), and interleukin-10 signaling (G) in the pathway.

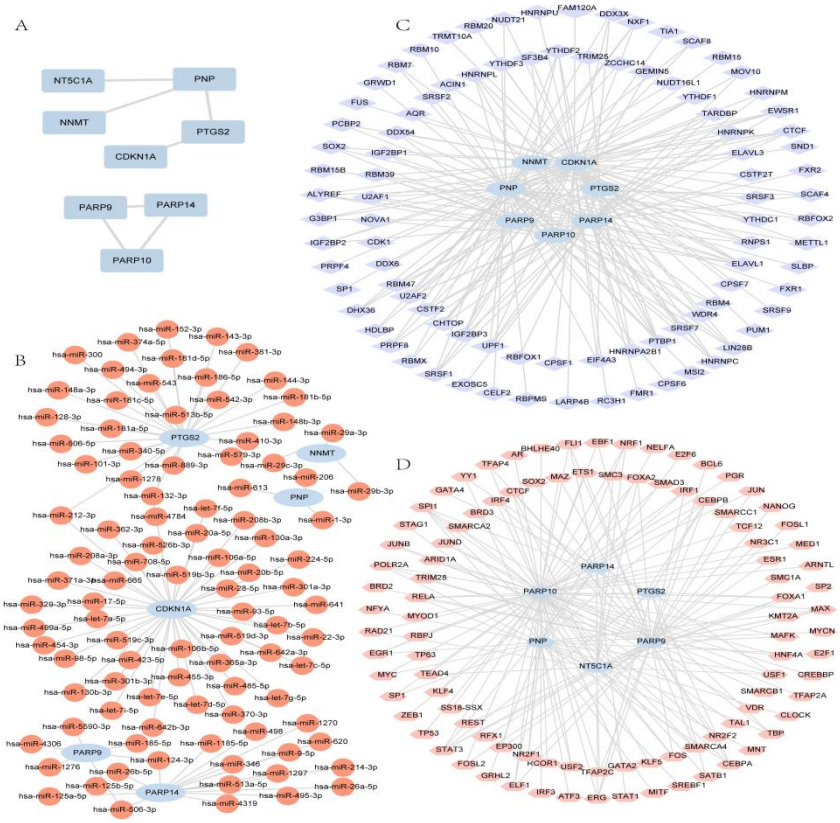

Fig. S7 Construction of protein-protein interaction network (PPI network), mRNA-miRNA, mRNA-RBP and mRNA-TF interaction network

(A) The protein interaction network (PPI network) of 8 key genes in the TCGA-GBMLGG dataset. (B) The mRNA-miRNA interaction network of key genes; the blue ovals represent mRNA; the orange-red dots represent miRNA. (C) mRNA-RBP interaction network; the blue ovals represent mRNA; the purple diamonds indicate RBPs. (D) mRNA-TF interaction network; the blue ovals represent mRNA; the pink hexagon blocks indicate TF.

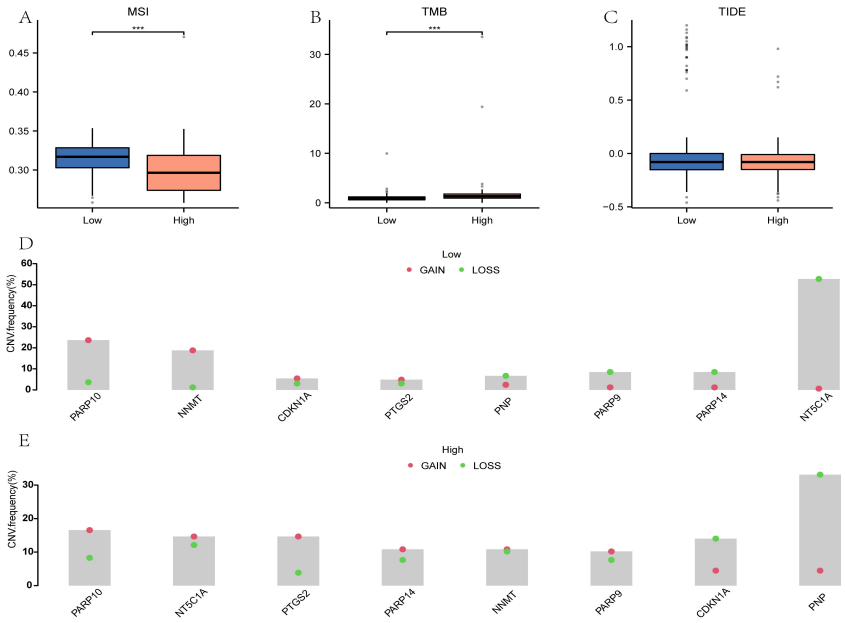

Fig.S8 CNV analysis and TMB, MSI, TIDE analysis of TCGA-GBMLGG dataset

(A-C) The comparison chart of key genes in terms of microsatellite instability (MSI)(A) , (B) tumor mutation burden (TMB)(B), TIDE immunotherapy score (C) between different groups based on NMRS. (D) CNV analysis of key genes in the low-risk group of the TCGA-GBMLGG data set key genes prognostic model. (E) CNV analysis of key genes in the high-risk group of the TCGA-GBMLGG data set key genes prognostic model. ***P < 0.001, very statistically significant.

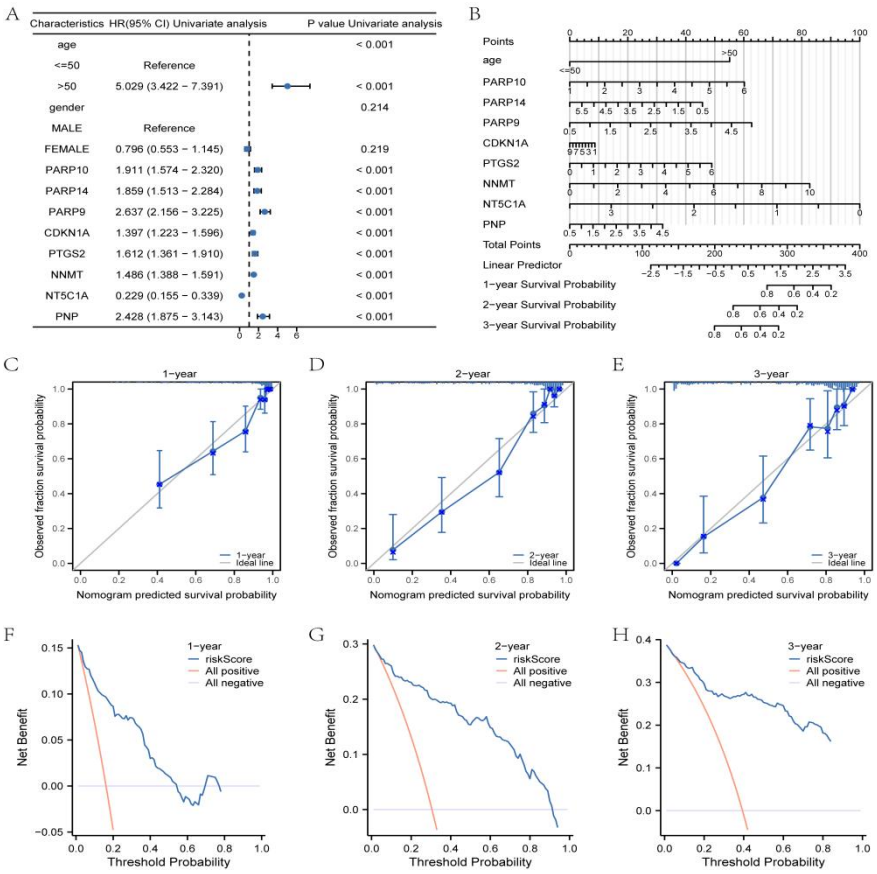

Fig. S9 Construction of multi-factor Cox regression model for TCGA-GBMLGG data set.

(A) Forest plot of the univariate Cox regression model for the TCGA-GBMLGG dataset. (B) Nomogram of multivariate Cox regression model. (C–E) 1-year (C), 2-year (D), and 3-year (E) calibration curves of multivariate Cox regression model nomogram analysis. (F–H) 1-year (F), 2-year (G), and 3-year (H) DCA plots of multivariate Cox regression models.